

# MULTI-SENSOR SIGNAL ACQUISITION AND DATA PROCESSING ANALYSIS OF COMBINE HARVESTER

## 联合收割机多传感器信号采集与数据处理分析

Wang Li <sup>1)\*</sup>, Li Shuo <sup>1)</sup>, Lv Dianji <sup>1)</sup>, Ekhlo Ghay <sup>2)</sup>

<sup>1)</sup> Beijing Institute of Economic and Management, Beijing / China

<sup>2)</sup> Exor Group, Amsterdam / Netherlands

\*Tel: 18330614933; E-mail: nw9836377laic@163.com

DOI: <https://doi.org/10.35633/inmateh-63-34>

**Keywords:** combine harvester, multi-sensor, signal acquisition, data processing

### ABSTRACT

In recent years, combine harvesters are increasingly developing in the direction of large-scale, technology, automation and intelligence, and more and more electrical equipment is installed on combine harvesters. The electrical system of combine harvester is prone to failure when it works in high temperature, high humidity, dusty and strong vibration environment. Parameters to be adjusted in the header system of combine harvester include header height, drum height, drum front and back position, cutting frequency and drum speed. Aiming at the inconvenience of debugging and testing the measurement and control system of combine harvester in the field operation environment, an intelligent control test bed of combine harvester was designed. The test bed can simulate various intelligent control algorithms of combine harvester in laboratory environment, control the forward speed of combine harvester according to data processing results, classify faults, and send and print stored data through serial communication. Experiments show that the system works stably and reliably, and can realize the integration of the monitoring system of combine harvester operation process. It can save costs and improve efficiency in the application of the monitoring system of combine harvester.

### 摘要

近年来,联合收割机日益向大型化、技术化、自动化和智能化方向发展,联合收割机上安装的电气设备越来越多。联合收割机在高温、高湿度、多灰尘和强振动环境中工作,其电气系统容易出现故障。联合收割机割台系统中需要调整的参数包括割台高度、滚筒高度、滚筒前后位置、滚筒速度、切割频率和滚筒速度。针对联合收割机测控系统在田间作业环境下调试和测试的不便,设计了一种联合收割机智能控制试验台。该试验台可以在实验室环境下模拟联合收割机的各种智能控制算法,根据数据处理结果,控制联合收割机的前进速度,进行故障分类处理,并通过串行通信发送和打印存储的数据。实验表明,该系统工作稳定可靠,能够实现联合收割机作业过程监控系统的一体化,在联合收割机测控系统的应用中能够节约成本,提高效率。

### INTRODUCTION

As an important tool of modern agriculture and an important material basis of agricultural mechanization, combine harvester has been rapidly developed and widely applied in recent years, and its development degree is related to the enhancement of agricultural productivity and the advancement of agricultural modernization in China (Chen X et al., 2019). At the same time, there are many problems in the actual use of the combine harvester (Chen Z et al., 2018). For example, when the forward speed of the combine harvester is not in harmony with the feeding amount, the threshing drum and the conveying trough are easy to be blocked. China is a big agricultural country with a long farming civilization, with a wide grain planting area. The rice planting area is nearly 33,000 square kilometres, accounting for about 1/4 of the total rice planting area in the world, which provides an important opportunity for the automatic harvest of agricultural machinery (Jih Y C et al., 2021). At present, the degree of automation and intelligence of the combine harvester in China is relatively low. Compared with the advanced combine harvester developed by foreign companies, there are still many problems and shortcomings.

Obtaining the yield information of crop plot and establishing the spatial distribution map of plot yield are the basis for realizing scientific control and investment and making management decision-making measures in the process of crop production (Yang Y et al., 2021).

Most of the models of combine harvesters developed in China at present are mainly small and medium-sized ones, which are suitable for local operation, but the automation degree of combine harvesters is increasingly difficult to meet the operation and use requirements of operators. In the process of combine harvester operation in China, the artificial subjective judgment is strong, the operation is cumbersome, and it depends on the daily accumulated experience and training technology of operators for adjustment and control, and the automation and intelligence are low, which seriously restricts the operation efficiency and development of combine harvester (Jin C *et al.*, 2019).

In this paper, a multi-sensor signal acquisition and processing system based on microprocessor C8051F020 is designed with a brand of tangential flow combine harvester as the experimental prototype. By analysing the working characteristics of the combine harvester and the working characteristics of each part, the monitoring objects of the system are selected, including cab, granary, header and threshing drum. On this basis, the software and hardware architecture is designed, including the selection of airborne front-end hardware platform and operating system, the selection of peripheral hardware modules, the implementation method of each software module and the design of information processing program, etc., which is used for simulating various intelligent control algorithms of the combine harvester.

Jeong *et al.* (Jeong W *et al.*, 2020) analysed the factors of header loss of combine harvester, and put forward a broken grain loss model based on linear statistical model. Based on theoretical mechanical analysis, the model function relationship between reel parameters and crop characteristics was constructed, and the header loss was collected through field experiments, which verified that the data fitting degree of the model was good. Hwang *et al.* (Yi Q *et al.*, 2021) used computer communication technology to package the traveling speed, grain yield, humidity, header lifting state, position information and other data acquired by the onboard data acquisition and processing unit of the harvester and transmit them to the monitoring centre through GSM terminal. Yuan C *et al.* (Ng KA *et al.*, 2019) measured the vibration of the bottom floor of the cab with YE6261B dynamic data acquisition tester to check the vibration resistance of instruments and meters. Japan Kubota Company has done a lot of research on small-sized combine harvesters, and designed an intelligent monitoring and control system by using sensing technology, display device and geographic information system, which was put into use on PRO208 combine harvester (Ryoei I *et al.*, 2021). In addition, Shuenn-Yuh *et al.* (Shuenn Y and Lee C. 2019), a foreign research scholar, designed an agricultural machinery telemetry application system based on OPC-UA standard, which used GPS, CAN-Bus and 3G technology to remotely obtain information such as driving speed, fuel oil, heading direction, crop moisture content and yield of the combine harvester.

## MATERIALS AND METHODS

### Overall design scheme

When the combine harvester operates in the field, the operators need to adjust the joystick constantly due to the harsh field environment, the fluctuation of terrain and the inconsistent crop growth. Most operators judge and adjust the joystick according to the harvest experience accumulated all the year round. Many mechanical joysticks are a severe test for the operators (Tasanai P J S *et al.*, 2021), so it is necessary to study and improve the control mode of the combine harvester.

The video monitoring system of combine harvester operation site is mainly composed of embedded airborne monitoring front-end system, remote indoor large-screen monitoring centre or hand held mobile monitoring terminal, and Internet of Things platform, as shown in Figure 1.

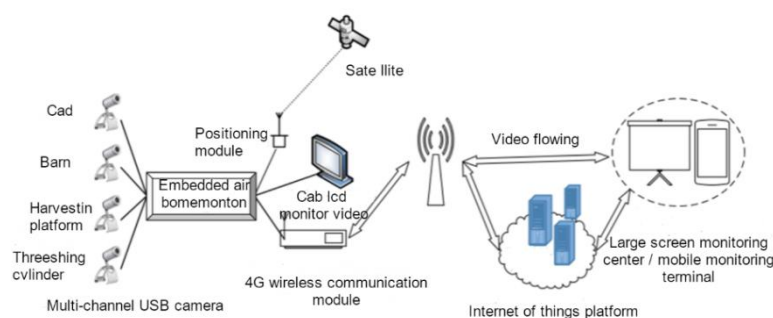


Fig. 1 - Overall scheme of system

The embedded airborne monitoring front-end system is installed and deployed on the combine harvester, which uses GPS module to locate the real-time position of the combine harvester, extracts, calculates and analyses the information of the positioning module, transmits the video image information to the remote indoor large-screen monitoring centre through 4G wireless network, and uploads the positioning information and image data to the Internet of Things platform. Users can log in to the internet of things platform through the mobile app or PC Web, access the image data of the job site of the combine harvester and know its geographical location in time.

### Hardware construction

The visual navigation platform is based on that hardware architecture of the USB bus structure of the vehicle-mounted computer (fig. 2), including the high-speed data collector NI 2 USB6211.

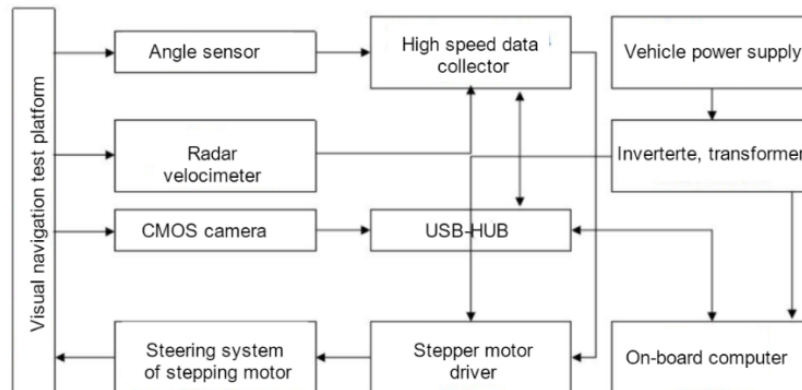


Fig. 2 - Hardware structure of visual navigation control system of combine harvester

The vehicle-mounted power supply is used to invert AC220V, boost voltage to obtain 24V, and DC2DC conversion to obtain 5V, which is convenient for the control system. NI2USB6211 provides 12 channels of A/D conversion, 2 channels of timers to generate pulses or count, and 4 channels of TTL/O, which are mainly used to collect angular displacement voltage and radar velocimeter speed signals, and generate pulse signals with specified frequency for stepper motor drivers (Moreno E et al., 2020) (Ng K A et al., 2019). All expansion circuits and boards are packaged in anti-interference metal box, and the interface adopts unified aviation plug mode, which is convenient for use in harsh environment to improve the stability of the system.

The control system is mainly used to control the forward speed of the test trolley, collect multi-channel rotational speed signals such as simulated roller and screw conveyor, and give alarm and display. FX3U-64MT PLC (Programmable Logic Controller) is selected as the intelligent control module, which integrates almost all analog and digital peripherals and other functional components required by the control system, and it also has powerful communication function. In the signal acquisition module, a plurality of corresponding multisensors are input into the controller through corresponding conditioning circuits to complete signal acquisition; The LCD (Liquid Crystal Display) module adopts HD104MK type display, and the acousto-optic alarm module prompts the fault type through the blinking of buzzer and LED (Light-Emitting Diode) lamp. The parameter setting module sets the parameters by 6 buttons: "Automatic", "Manual", "Screen Control", "+", "-" and "Confirm" (Jin C et al., 2018).

The detection of the speed and forward speed of the reel of the combine harvester belongs to the field of speed measurement. Commonly used speed measurement methods are: magnetolectric speed measurement method, magnetic sensitive speed measurement method, capacitive speed measurement method, pulse number speed measurement method, etc. Considering the harsh working environment of the combine harvester, which is affected by water, grease, dust and vibration, the photoelectric and capacitive multi-sensors are easy to bring measurement errors. In this paper, the magnetolectric multi-sensors are selected for speed measurement.

The main working principle of magnetolectric Haldore sensor is to detect the magnetic field with polar magnetic steel and send out pulse signals, which are sent to the controller for subsequent processing after being shaped (Qiao N et al., 2020).

Because the controller adopts PLC, which has high anti-interference ability, the signal at the input end is connected to the internal LED lamp of the photoelectric coupler, and the photoelectric tube of the photoelectric coupler receives the input signal, which can realize reliable transmission with external signals (Rahman M et al., 2019). The detection principle is shown in Figure 3.

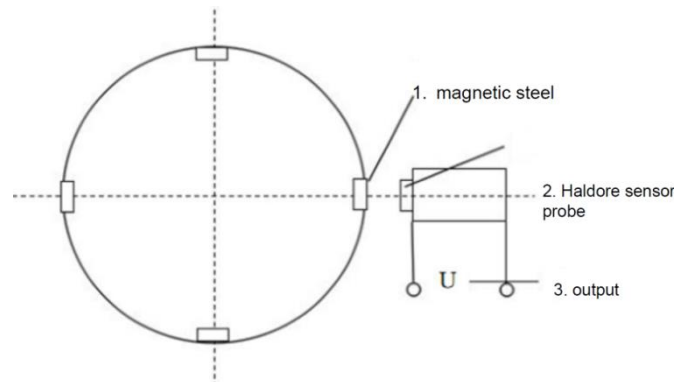


Fig. 3 - Detection principle of Haldore sensor

The pulse signal sent by Haldore sensor has poor waveform edge in actual acquisition. In order to better acquire the signal waveform of Haldore sensor, filter and shape the signal, the circuit design is shown in Figure 4.

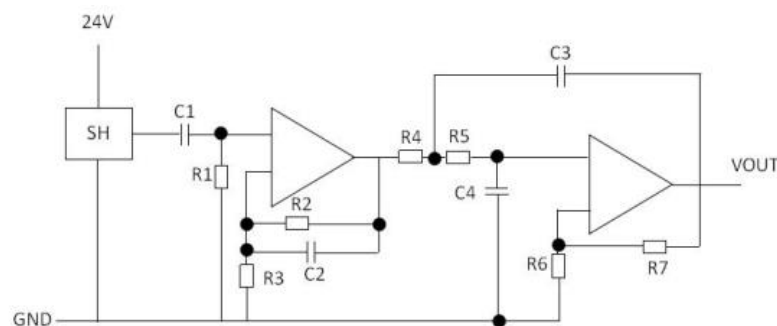


Fig. 4 - Design drawing of Haldore sensor signal acquisition circuit

**Fuzzy PID algorithm**

The working condition of combine harvester is complex, and the adjustment of reel speed is easily affected by machine vibration and inertia. The stability of control system constructed by conventional PID control method is poor. The three coefficients of conventional PID controller need to be adjusted manually, and it is difficult to meet the system control requirements with strong time variability. To obtain satisfactory control effect, it is necessary to continuously adjust the three coefficients of PID controller online. PID control, also known as PID regulation, is a mature and widely used control system with simple principle, convenient structure, flexibility, high efficiency and easy adjustment. It consists of three parts: proportional control unit (P), integral control unit (I) and differential control unit (D).

Fuzzy PID controller is composed of fuzzy controller and PID regulator. Deviation  $e$  and deviation change rate  $\Delta e$  are the input variables of fuzzy controller. Then, according to fuzzy control rules, logic reasoning and defuzzification are carried out, and three adjustment coefficients  $k_p, k_i, k_d$  of the controller are adjusted online. The linear combination of them constitutes the actual control quantity, which controls the output of the controlled object.

Set  $u(t)$  as the output during  $t$  sampling,  $e(t)$  as the deviation during  $t$  sampling period,  $T$  as the sampling period, and the calculation formula of output control quantity is:

$$u(t) = k_p e(t) + k_i T \sum_{i=1}^t e(t_i) + k_d [e(t_i) - e(t_{i-1})] \tag{1}$$

The formula for calculating the speed deviation  $e(t)$  of reel at time  $t$  and the rate of deviation change  $\Delta e$  is as follows:

$$e(t_i) = n_i - n_i' \tag{2}$$

$$\Delta e = \frac{e(t_i) - e(t_{i-1})}{t_i - t_{i-1}} \tag{3}$$

Where  $n_i$  is the target value of reel speed  $n_i$  is the current sampling value of reel speed.

**Control quantity of navigation controller**

In order to make the navigation controller speed adaptive, the influence of driving speed on the control quantity  $u$  must be considered. Therefore, through the preliminary road test research, the control gain  $K$  of the controller, a control period  $T$ , the distance  $\zeta$  travelled in the control period, the relationship between the processing frame number  $\Gamma$  and the driving speed  $v$  in the control period are analysed.

In order to improve the rapid response capability of the controller, the  $PD$  controller is designed, and the calculation formula of the control quantity  $u_k$  of the computer control system is (Cai H Y et al., 2021):

$$u_k = K(\zeta_p e_k + \zeta_d \dot{e}_k) \tag{4}$$

Where:

$e_k, \dot{e}_k$ ——Current navigation path deviation and deviation change rate;

$\zeta_p, \zeta_d$ ——Proportional coefficient and differential coefficient;

$K$ ——Scale factor, which is equivalent to the gain of the system.

Setting  $\zeta_p + \zeta_d = 1$ , these two coefficients directly determine the effect of deviation and deviation change rate. Based on the experience of manual driving, fuzzy design method is adopted, which is described in detail in reference (Song X.J. 2019) and will not be repeated.

The navigation path parameters detected by vision are converted into the current heading deviation  $\theta_k$  and dead-end deviation  $d_k$ . According to the analysis of navigation path detection error in literature (Xu L et al., 2019), when the angle is small, the angle detection error is better than the intercept detection error, so the deviation  $e_k$  is:

$$e_k = \begin{cases} (\theta_k - \theta_o) / \theta_m & (\theta_k \geq \delta \text{ or } \theta_k \leq -\delta) \\ (d_k - d_o) / d_m & (-\delta < \theta_k < \delta) \end{cases} \tag{5}$$

Where:

$\theta_o, d_o$ ——Target heading angle and target dead position deviation;

$\theta_m, d_m$ ——Maximum value of heading deviation and dead position deviation;

$\delta$ ——The allowable threshold of course deviation is obtained from the test.

**Software design**

Collection and processing of feeding amount and loss amount are completed in serial port interrupt 0. The baud rate of serial port initialization configuration is 115 200 b/s, and the serial port sending protocol is shown in Figure 5.

|                               |             |   |      |          |
|-------------------------------|-------------|---|------|----------|
| Preamble                      | MID         | LEN   | DATA | Checksum |
| Description of the agreement: |             |   |      |          |
| Field                         | Field width | Discription   |      |          |
| Preamble                      | 1 Byte      | Instruct development to send one frame of data (0xFA)                               |      |          |
| MID                           | 1 Byte      | The frame information ID indicates the transmitted frame type                       |      |          |
| LEN                           | 1Byte       | Data length (fixed at 8 bytes in case of double)                                    |      |          |
| DATA                          | LEN Byte    | Data (the number of data sent depends on the size of LEN)                           |      |          |
| Checksum                      | 1 Byte      | Check bit: subtract all transmissions except the frame header with zeroSum of bytes |      |          |

Fig. 5 - Serial port sending protocol

At first, the received byte is judged by serial port interruption, if it is 0xFA, then 11 bytes of DATA received subsequently are put into the array R Data (Yan L *et al.*, 2021), and these 11 bytes of data are summed and verified. After the verification is passed, the MID bit is judged, if MID is 0x00, it is the feeding amount signal, and the data is processed, and the result is put into the global variable; If MID is 0x01, it is a loss signal. Data is processed, and the result is put into the global variable. The dynamic digital display subroutine in the main program realizes the dynamic refresh of feeding amount and loss amount by processing these two global variables.

The test bed adopts different algorithms for different tests, which can optimize the selection of algorithms. Fig. 6 is the subroutine flow of multi-information fusion fuzzy control algorithm for controlling forward speed (Zhang Z G *et al.*, 2019).

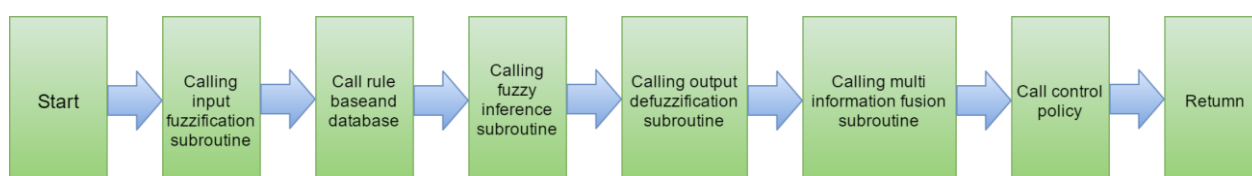


Fig. 6 - Multi-information fusion fuzzy control algorithm subroutine flow chart

The subroutines of multi-information fusion fuzzy control algorithm are as follows: calling input fuzzification subroutine, calling rule base and database, calling fuzzy inference subroutine, calling output fuzzification subroutine, calling multi-information fusion subroutine and calling control strategy. Then, according to the algorithm results, it is judged whether the forward speed needs to be adjusted, and if so, the stepper motor control subroutine is called to reasonably adjust the forward speed, thus completing the intelligent control of the forward speed of the combine harvester. At the same time, the test bench can adopt different control algorithms for the same test, for example, the forward speed can also adopt grey prediction fuzzy control algorithm (Chavdar V *et al.*, 2021).

## RESULTS

### Data acquisition experiment

Table 1 shows the parameters such as forward speed, conveying trough rotation speed, drum rotation speed, header screw conveyor rotation speed, feed rate and loss rate collected under normal working conditions of the test bench. The results show that the data collected by the test bed is accurate and reliable.

Table 1

Data acquisition results

| Time<br>(s) | Speed of advance<br>(r·min <sup>-1</sup> ) | Rotating speed of drum<br>(r·min <sup>-1</sup> ) | Rotating speed of conveying trough<br>(r·min <sup>-1</sup> ) | Rotating speed of header auger<br>(r·min <sup>-1</sup> ) | Feeding amount<br>(kg·s <sup>-1</sup> ) | Loss rate<br>(%) |
|-------------|--|--|--|--|---|------------------|
| 0           | 0.3  | 720  | 336  | 155  | 4.2                                     | 0.41             |
| 1           | 0.3  | 720  | 320  | 160  | 4.0                                     | 0.44             |
| 2           | 0.3  | 720  | 305  | 140  | 4.3                                     | 0.39             |
| 2           | 0.3  | 714  | 307  | 150  | 3.9                                     | 0.45             |
| 4           | 0.3  | 711  | 325  | 152  | 3.8                                     | 0.41             |
| 5           | 0.3  | 696  | 310  | 145  | 4.0                                     | 0.41             |
| 6           | 0.3  | 716  | 327  | 161  | 4.2                                     | 0.50             |
| 7           | 0.4  | 682  | 311  | 153  | 3.8                                     | 1.46             |
| 8           | 0.4  | 693  | 308  | 155  | 3.9                                     | 0.44             |
| 9           | 0.4  | 701  | 317  | 140  | 4.1                                     | 0.51             |
| 10          | 0.3  | 708  | 303  | 146  | 4.0                                     | 0.46             |

### Error analysis of cutting width setting

When setting the cutting width, if the set value is larger than the actual value, the calculated plot area is larger than the actual harvest area, which further leads to the output value of this point being smaller than the actual value, and the low-yield point will appear on the output map.



If it is less than the actual value, the high-yield point will appear on the yield map. In this way, the cutting width is set according to the observation of the harvester operator, and the operator must modify the cutting width according to the actual situation. The usual method is to eliminate these data which are not satisfied with the cut width records, because the data points collected by the harvester are very dense, it will not have much influence on the final yield distribution map.

Table 2

| Data column | Number of Production points | Maximum output (kg·hm <sup>-2</sup> ) | Minimum yield (kg·hm <sup>-2</sup> ) | Average output (kg·hm <sup>-2</sup> ) |
|-------------|-----------------------------|---------------------------------------|--------------------------------------|---------------------------------------|
| 1           | 80                          | 5532                                  | 778                                  | 4120                                  |
| 2           | 79                          | 4780                                  | 2566                                 | 3860                                  |
| 3           | 36                          | 8933                                  | 1890                                 | 6250                                  |
| 4           | 69                          | 3560                                  | 2310                                 | 3571                                  |
| 5           | 70                          | 3917                                  | 2428                                 | 3690                                  |

In the harvesting process, a series of high-yield points appeared in the original data table because the cutting width set by visual inspection at that time was smaller than the width of crops actually entering the header. In Table 2, the data in this column is compared with the adjacent columns, and the output varies greatly. The average output of this column is 6250 kg·hm<sup>-2</sup>, while the average output of adjacent columns is less than 412 kg·hm<sup>-2</sup>. The header width of the combine harvester is 6m, so the interval between two adjacent columns of data is about 6m. However, the output data cannot change greatly in a small range, so there are errors in this column of data.

## Vibration acceleration

### Test 1

Install acceleration multi-sensors in horizontal direction, vertical direction and axial direction in the middle frame position of the header of the combine harvester, and start collecting and saving data after the engine of the combine harvester accelerates to run stably, as shown in Table 3.

Table 3

| Condition           | Direction            | Experiment serial number |       |       |       |       |
|---------------------|----------------------|--------------------------|-------|-------|-------|-------|
|                     |                      | 1                        | 2     | 3     | 4     | 5     |
| Working condition 1 | Horizontal direction | 0.124                    | 0.178 | 0.171 | 0.169 | 0.166 |
|                     | Normal direction     | 0.141                    | 0.122 | 0.142 | 0.138 | 0.130 |
|                     | Axial                | 0.136                    | 0.130 | 0.133 | 0.136 | 0.134 |
| Working condition 2 | Horizontal direction | 2.150                    | 2.514 | 2.529 | 2.551 | 2.530 |
|                     | Normal direction     | 2.036                    | 1.948 | 2.014 | 2.058 | 2.026 |
|                     | Axial                | 1.966                    | 1.902 | 1.963 | 1.984 | 1.985 |

The two working conditions of this test are: only the engine rotates at the big throttle (working condition 1), and the big throttle of the engine runs together with the cutter transmission system (working condition 2). Judging from the data, the vibration of the header in the horizontal direction is the largest. The maximum acceleration in horizontal direction is 0.178 when the big throttle engine rotates, and 2.551 when the big throttle engine runs together with the cutter transmission system.

### Test 2

In this test, the horizontal vibration conditions of the three positions near the cutter, the frame above the header shield and the header bridge at the same time are measured, and the data under different working conditions are shown in Table 4. The working conditions are small throttle rotation (working condition 1), middle throttle rotation (working condition 2), big throttle rotation (working condition 3), big throttle rotation, cutter transmission system (working condition 4) and middle throttle 2-gear traveling transportation state (working condition 5).

Table 4

| Test 2 - Vibration acceleration            |                          |                   |       |       |       |       |
|--|--------------------------|-------------------|-------|-------|-------|-------|
| Location                                   | Experiment serial number | Working condition |       |       |       |       |
|  |                          | 1                 | 2     | 3     | 4     | 5     |
| Near the cutter                            | 1                        | 0.022             | 0.021 | 0.428 | 1.569 | 0.033 |
|  | 2                        | 0.011             | 0.024 | 0.021 | 1.669 | 0.043 |
|  | 3                        | 0.025             | 0.026 | 0.368 | 1.718 | 0.039 |
| Frame above shield                         | 1                        | 0.145             | 0.139 | 0.166 | 2.556 | 0.203 |
|  | 2                        | 0.106             | 0.120 | 0.184 | 2.690 | 0.196 |
|  | 3                        | 0.151             | 0.137 | 1.77  | 2.714 | 0.188 |
| The harvesting platform crosses the bridge | 1                        | 0.081             | 0.162 | 0.225 | 2.512 | 0.223 |
|  | 2                        | 0.096             | 0.177 | 0.206 | 2.501 | 0.310 |
|  | 3                        | 0.088             | 0.180 | 0.329 | 2.886 | 0.281 |

Through data analysis, it is concluded that the vibration of the header is the largest at the bridge position, with the maximum horizontal acceleration of 2.886, followed by the frame above the header shield and the smallest near the cutter.

#### Study on the correlation between manual determination of particulate impurities and multi-sensor determination of particulate impurities

By adjusting the advancing speed, calibration experiments were carried out in the field, and different rheological properties of materials were obtained. The test temperature is 18°C and the ambient humidity is 68%. Experiments were carried out at three different forward speeds of 0.6, 1.0 and 1.3 m/s, which were related to the feed speeds of 1.5, 2.0 and 2.3kg/s, respectively. The quantity and discharge speed of grain and non-grain materials discharged from grain box auger are affected by their rheological properties, which largely depend on the output of combine harvester. Therefore, the forward speed of the combine harvester is set to three levels to obtain different rheological properties of materials, and the sampling device is installed below the outlet of the diversion tunnel of the granary.

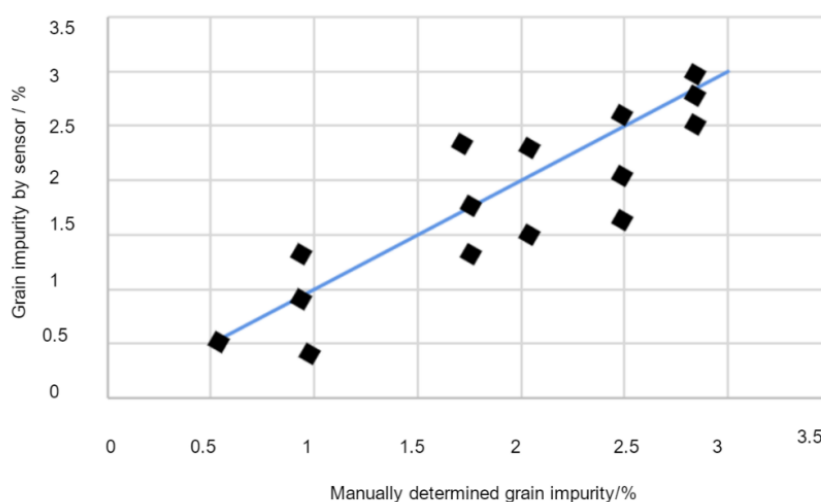


Fig. 7 - Correlation between manual determination of grain impurities and multi-sensor determination of grain impurities

In order to verify the influence of different grain impurities on the image, the same event was shot at different straw levels. It is observed that with the control of grain impurities, the average number of straw in the visual window increases; However, because the clarity of the image depends on the brightness of the image, the influence of illumination is easily ignored. By analysing the relationship between multi-sensor and manual determination of impurities, a correlation was found, as shown in Figure 7.



## CONCLUSIONS

This paper designs the overall scheme of combine video monitoring system, analyses the working process of combine, and selects the monitoring object of the system. According to the overall scheme of the system, the appropriate embedded hardware and software platform and peripheral hardware modules are selected, and the overall hardware architecture and software architecture of the system are designed completely. The designed double closed-loop PD controller can effectively change the control parameters dynamically according to the change of driving speed. The motor module is used to simulate the rotation speed of the combine drum, conveyor trough, header screw conveyor and other rotating parts, and the simulation module is used to simulate the feeding process and loss process. The intelligent control algorithm of the forward speed of the test bed is tested, and the expected effect is achieved. Although the anti-interference measures such as filtering and shaping are used in the circuit design, it will still interfere with the signal acquisition of the whole system. We can consider sending information to the controller through the industrial bus to improve the anti-interference and stability of the whole system.

## REFERENCES

- [1] Cai H.Y., Li F.Z., Lv P., Ran L.J., Zou L.D., (2021). Intelligent aquaculture environment monitoring system based on lora communication technology. *INMATEH Agricultural Engineering*, Vol.63, Issue 01, pp.109-120. Romania;
- [2] Chavdar V., Atanas A., Valentin V., (2021), Calculation of field capacity and fuel consumption of mobile machinery with bunkers, tanks or other containers for agricultural goods. *INMATEH Agricultural Engineering*, Vol.63, Issue 01, pp.19-28. Romania;
- [3] Chen X., Wu C.Y., Sharla C., (2019). Design and research of grain combine harvester yield measurement system. *Chinese Journal of Agricultural Machinery Chemistry*, Vol.40, Issue 308-10, pp.26-30. China;
- [4] Chen Z., Wu H.C., Zhang Y.H., (2018), Development of automatic depth limiting system for semi-fed four-row peanut combine harvester. *Journal of Agricultural Engineering*, Vol.34, Issue 15, pp.18-26. China;
- [5] Jeong W., Tsingas C., Almubarak M.S., (2020). A numerical study on deblending of land simultaneous shooting acquisition data via rank-reduction filtering and signal enhancement applications. *Geophysical Prospecting*, Vol.68, Issue 6. United Kingdom;
- [6] Jhih Y.C., Hsin C.C., Chih W.C., Kai M.Y., (2021), Relationship between Antioxidant Components and Oxidative Stability of Peanut Oils as Affected by Roasting Temperatures. *MDPI (Agriculture)*, Vol. 11, Issue 004, pp. 300. Switzerland;
- [7] Jin C., Lian Y., Li Y.M., (2019). Design of sampling box for rice impurity rate sensor in grain bin of combine harvester. *Journal of Agricultural Engineering*, Vol.035, Issue 005, pp.18-25. China
- [8] Jin C., Wang Y.H., Lian Y., (2018). Development of on-line monitoring device for grain moisture content of high-frequency capacitive combine harvester. *Journal of Agricultural Engineering*, Vol.34, Issue 10, pp.36-45. China;
- [9] Tasanai P.J.S., Maliwan N., Somjit H., Phithak I., Anupan K.K., (2021). Production and Molecular Identification of Interspecific Hybrids between *Phaius mishmensis* (Lindl. and Paxton) and *Phaius tankervilleae* (Banks) Blume. *MDPI (Agriculture)*, Vol. 11, Issue 004, pp. 306. Switzerland;
- [10] Moreno E., Jess J., Morales M.O., Tejeida P.R., (2020). Biomedical Signal Acquisition Using Sensors under the Paradigm of Parallel Computing. *Sensors*, Vol.20, Issue. 23, p.6991. Switzerland;
- [11] Ng K.A., Yuan C., Rusly A., (2019), A Wireless Multi-Channel Peripheral Nerve Signal Acquisition System-on-Chip. *IEEE Journal of Solid-State Circuits*, Vol.54, Issue 99, pp.2266-2280. United States;
- [12] Ng K.A., Yuan C., Rusly A., (2019), A Wireless Multi-Channel Peripheral Nerve Signal Acquisition System-on-Chip. *IEEE Journal of Solid-State Circuits*, Vol.54, Issue 99, pp.2266-2280. United States;
- [13] Qiao N., Wang L., Zhu W., (2020). An improved path-tracking controller with mid-angle adaptive calibration for combine harvester. *Journal of Instrumentation*, Vol.15, Issue 01, P01025. United Kingdom;
- [14] Rahman M.M., Ishii K., Noguchi N., (2019), Optimum harvesting area of convex and concave polygon field for path planning of robot combine harvester. *Intelligent Service Robotics*, Issue 24, pp.1-13. Germany;
- [15] Ryoei I., Takamitsu K., (2021), Development of paddy-field water level gage corresponding to a sensor-network. *INMATEH Agricultural Engineering*, Vol.63, Issue 1, pp.131-136. Romania;

- [16] Shuenn Y., Lee C., (2019). Ultra-High-Frequency Radio-Frequency-Identification Baseband Processor Design for Bio-Signal Acquisition and Wireless Transmission in Healthcare System. *IEEE Transactions on Consumer Electronics*, Vol.66, Issue 1, pp.77-86. United States;
- [17] Song X.J., (2019), A brief description of multi-sensor data processing and fusion. *Science and information technology*, Vol.000, Issue 003, pp.21-21. China;
- [18] Xu L., Wei C., Liang Z., (2019), Development of rapeseed cleaning loss monitoring system and experiments in a combine harvester - ScienceDirect. *Biosystems Engineering*, Issue 178, pp.118-130. United States;
- [19] Yang Y., Chun R.Q., Wan R.G., Cai F.L., (2021), Responses of root characteristic parameters and plant dry matter accumulation, distribution and transportation to nitrogen levels for spring maize in Northeast China. *MDPI(Agriculture)*, Vol.11, Issue 4, p.308. Switzerland;
- [20] Yi Q., Dai X.F., Chen Z., Dai N.Z., Mi L.K., (2021). Numerical simulation and experimental study of inner flow field of seed pelleting premixer in spouted fluidized bed. *INMATEH Agricultural Engineering*, Vol.63, Issue 1, pp.241-248. Romania;
- [21] Yan L., Xiao D.S., Jin W., Qiang D., Chao Y.W., Chun B.D., Tian L., (2021). Effects of nitrogen application rate on protein components and yield of low-gluten rice. *MDPI (Agriculture)*, Vol.11, Issue 4, pp.302. Switzerland;
- [22] Zhang Z.G., Peng C., Sun Y.F., (2019). Signal analysis and processing of feed monitoring system of combine harvester. *Journal of Agricultural Machinery*, Vol.50, Issue S1, pp.80-85. China.